RSC Advances

ROYAL SOCIETY OF CHEMISTRY

www.rsc.org/advances

Journal Name

RSCPublishing

COMMUNICATION

Facile Synthesis of Bismuth Oxide/Bismuth Vanadate Heterostructures for Efficient Photoelectrochemical Cells

Cite this: DOI: 10.1039/x0xx00000x

Received 00th January 2012,
Accepted 00th January 2012

DOI: 10.1039/x0xx00000x

www.rsc.org/

Kai-Hang Ye,[a] Xiang Yu,[ab] Zhiguang Qiu,[a] Yi Zhu,[a] Xihong Lu[c] and Yuanming Zhang [a,*]

Herein, we report a facile approach to synthesize the $Bi_2O_3/BiVO_4$ heterostructures for photoelectrochemical (PEC) cells. Due to the fast separation of the electron-hole pairs as a result of the p-n junction, the $Bi_2O_3/BiVO_4$ heterostructures achieved a remarkable photocurrent of 2.58 mA cm^{-2} at 1.2 V vs. Ag/AgCl, which is about 5 times than the pristine $BiVO_4$.

Due to ever-growing environmental concerns and increasing energy demands, hydrogen is considered as a key energy of the future because of its clean, renewable, carbon-free, and high energy density properties.[1-6] Inspired by natural photosynthesis, artificial photoelectrochemical (PEC) water splitting is a promising pathway to produce economically hydrogen. [7-10] The efficiency of PEC water splitting is largely determined by the properties of the photoelectrode, and considerable efforts have been devoted to exploring the highly active photoelectrode materials. Semiconductor metal oxides such TiO_2,[11] ZnO, [12-14] Fe_2O_3, [15] In_2O_3, [16] and WO_3 [17] have been extensively studied as photoanodes for PEC water splitting and numerous successes have achieved. Among various metal oxides, binary metal oxide $BiVO_4$ hold great promise for its significant advantages of the photoactive phase i.e. the monoclinic scheelite phase with a band gap of ~2.36 eV and high theoretical efficiency of 9.1%, which is capable of harvesting visible light. [9, 18, 19] Nevertheless, the efficiency of the $BiVO_4$ is still low as a result of its relatively poor light-harvesting ability and rapid recombination of photo-generated carriers. [20-22] Therefore, it is highly desirable and important to improve the photoactivity and of $BiVO_4$ by increasing the efficiency of absorption of the $BiVO_4$ and the separation of the electron-hole pairs.

To improve the PEC activity of $BiVO_4$ photoanodes, some strategies including element-doping, hydrogenation and composites have been proposed. Another effective strategy is to develop $BiVO_4$-based heterostructures. For example, various heterostructures such as $WO_3/BiVO_4$, [23] $CaFe_2O_4/BiVO_4$,[24] $TiO_2/BiVO_4$ [25] and $BiVO_4/Bi_2S_3$ [26] have been reported and enhanced PEC activity of these photoanodes haven been achieved as a result of the increased carrier density, reduced electron-hole recombination and the narrow band gap of the semiconductor. However, the present PEC performance of these heterostructures is still unsatisfactory. [3] Therefore, the development of new $BiVO_4$-based heterostructure photoanodes with high PEC activity and excellent stability is very desirable.

In this work, we firstly reported the design and synthesis of the $Bi_2O_3/BiVO_4$ p-n heterostructures for efficient PEC cells. α-Bi_2O_3 is an intrinsic p-type semiconductor with good PEC water splitting and photocatalytic activity [27]. When the p-type Bi_2O_3 and n-type $BiVO_4$ are integrated together, a number of p-n junctions will be formed. Then, the holes in the valence band (VB) of the p-type Bi_2O_3 will combine with the electrons in the conduction band (CB) of the n-type $BiVO_4$ due to the p-n junctions. As a consequence, the photoexcited electron-hole pairs are effectively separated by this novel n-p junction structure, which is crucial for the enhancement of PEC activity. Our results show that the $Bi_2O_3/BiVO_4$ p-n heterostructures achieved a remarkable photocurrent density of 2.58 mA cm^{-2} at 1.2 V vs. Ag/AgCl, which is about 5 folds that of pristine of $BiVO_4$. The Incident-photon-to-current-conversion efficiency (IPCE) of $Bi_2O_3/BiVO_4$ reaches 35.6% at 440 nm, which is much higher than that of the pristine $BiVO_4$ (about 10% at 440 nm). The Mott-Schottky analysis supports that the $Bi_2O_3/BiVO_4$ electrode possesses one order of magnitude improvement on donor density compared to the bare $BiVO_4$ electrode. This high photocatalytic activity makes $Bi_2O_3/BiVO_4$ a promising and an active photoanode.

The $Bi_2O_3/BiVO_4$ heterostructure nanospheres were prepared on FTO substrates *via* a two-step process, as schematically illustrated in Figure 1. Metallic Bi nanobelts were firstly grown on FTO substrates by electrodeposition (experimental section). As shown in Figure 1b, the deposited film is black in colour and consisting of nanobelts with a 300 nm wide dendritical structure. XRD spectrum confirms that the deposited film is rhombohedral Bi (Figure S4a and Figure S5). To obtain the $Bi_2O_3/BiVO_4$ heterostructures, the as-prepared Bi nanobelts were impregnated in the solution of 0.1 mol L^{-1} NH_4VO_3 for 6 h and then annealed at 550 ^oC in air (experimental section). Interestingly, the colour of the film has been changed from black to yellow (inset in Figure 1c), and XRD studies clearly demonstrate the successful

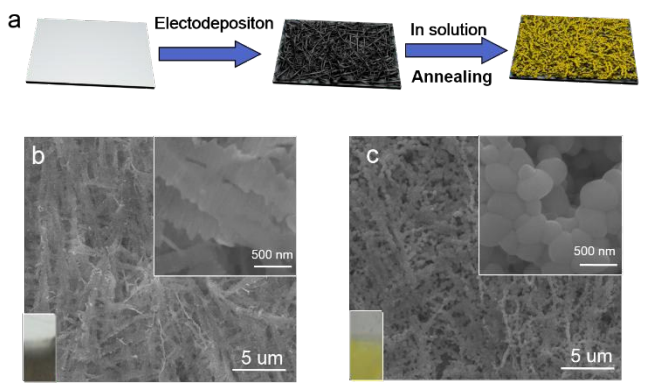

Figure 1. (a) Schematic diagrams for the growth process of $Bi_2O_3/BiVO_4$ heterostructures, SEM images of (b) Bi, (c) $Bi_2O_3/BiVO_4$ heterostructures.

transformation from metallic Bi to $Bi_2O_3/BiVO_4$ (Figure S4d). As shown in Figure 1c, the dendritical structure is basically retained after formed the $Bi_2O_3/BiVO_4$ heterostructures. Additionally, it should be noted that the Bi nanobelts have been transformed into some connected nanospheres with a dendritical structure. Furthermore, the composition of the $Bi_2O_3/BiVO_4$ heterostructures can be readily adjusting the immersion time in the NH_4VO_3 solution. For example, $Bi_2O_3/BiVO_4$ heterostructures was obtained when the immersion time was fixed to 6 h, as shown in Figure S1. When the immersion time increased to 12 h, pure $BiVO_4$ nanospheres were obtained (Figure S2 and Figure S4c). In addition, pure Bi_2O_3 nanobelts could be formed by directly annealed the as-prepared Bi nanobelts in air (Figure S3 and Figure S4b). All these results clearly show that our present method is an effective method to synthesize the heterostructures with controllable composition. More XRD details of Bi_2O_3, $BiVO_4$, and composite were shown in Figure S4.

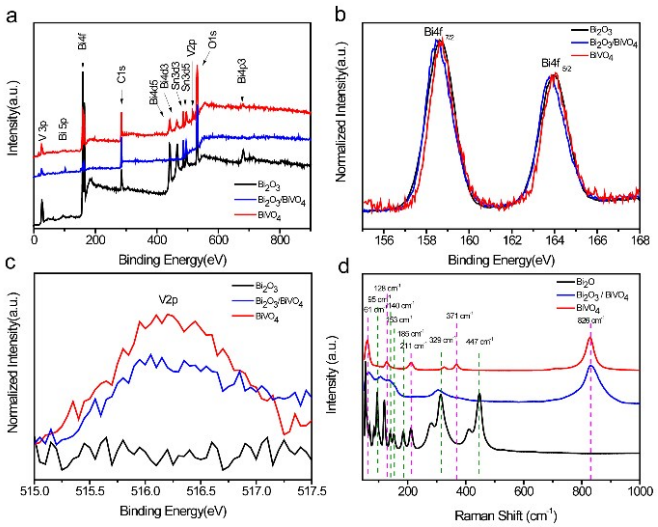

Figure 2. (a) Survey XPS spectra and high-resolution XPS spectra of Bi_2O_3, $Bi_2O_3/BiVO_4$ heterostructures and $BiVO_4$. XPS spectra of (b) Bi_{4f} (c) V_{2p}. (d) Enlarged Room temperature Raman-scattering spectrum in range 50-800 cm^{-1} of Bi_2O_3, $Bi_2O_3/BiVO_4$ heterostructures and $BiVO_4$.

In order to further investigate the chemical composition and defect state of the products, X-ray photoelectron spectroscopy (XPS) analysis was performed. The XPS survey spectra collected for the pristine Bi_2O_3, $BiVO_4$ and $Bi_2O_3/BiVO_4$ heterostructures were shown in Figure 2a. Besides Sn, Si signals originating from the FTO substrate and C signals originating from the adventitious carbon, only Bi, V and O are detected on the sample surface. Figure 2b shows the Bi 4f XPS spectra of the samples. The doublet broad peaks with higher binding energy of 159.4 eV and 164.6 eV are observed for all the samples, which are consistent with the characteristic Bi $4f_{7/2}$ and Bi $4f_{5/2}$ of Bi^{3+} peaks[28]. This reveals that the Bi has been successfully converted into Bi^{3+}. Moreover, the V 2p spectra confirm the presence of V^{5+} in the $Bi_2O_3/BiVO_4$ and $BiVO_4$ samples (Figure 2c). The binding energies of the synthetic peaks centred at 516.3 eV are consistent with the reported values for V^{5+} [29]. Figure 2d displays the Raman spectra of Bi_2O_3, $Bi_2O_3/BiVO_4$ and $BiVO_4$. The peaks located at 329 cm^{-1} and 447 cm^{-1} are the characteristic peaks for Bi_2O_3 [30], while the peaks at 826 and 128 cm^{-1} are assigned to the V-O vibration of $BiVO_4$ structure units [30]. For the $Bi_2O_3/BiVO_4$ sample, the peak at 826 cm^{-1} is assigned to $BiVO_4$ and the peak at 329 cm^{-1} is assigned to Bi_2O_3, respectively. Therefore, the $Bi_2O_3/BiVO_4$ sample consists of Bi_2O_3 and $BiVO_4$, which also affirmed the successful formation of the heterostructure.

In order to better understand the microstructure of $Bi_2O_3/BiVO_4$ heterostructures, transmission electron microscopy (TEM) analysis was carried out. Figure 3a is a typical TEM image of the as-prepared $Bi_2O_3/BiVO_4$ heterostructures, showing that a lot of nanoparticles of 5 nm in diameter are uniformly covered onto the surface of the spheres. Figure 3b shows the high-resolution TEM (HRTEM) image of the sample, suggesting the $Bi_2O_3/BiVO_4$ heterostructure nanospheres are well crystalline. The well-resolved lattice fringes of 0.32 nm that corresponding to the (120) plane of monoclinic Bi_2O_3 are well observed. The lattice fringes of 0.29 nm that corresponding to the (040) plane of monoclinic $BiVO_4$ are also observed. Therefore, the $Bi_2O_3/BiVO_4$ heterostructures are successfully prepared. As shown in Figure 3c-f, distributions of Bi, V and O are clearly presented by the STEM EDS elemental maps, which indicate that the Bi, V and O are uniformly embedded in the nanospheres, and high combining degree of each other.

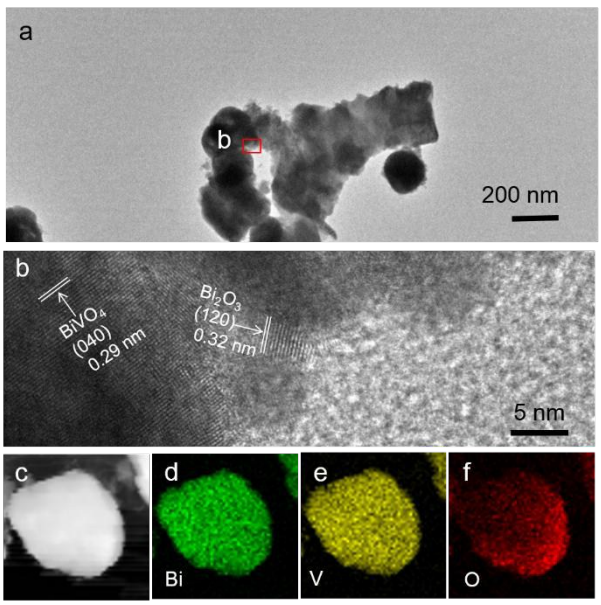

Figure 3. (a, b) TEM bright field images of the $Bi_2O_3/BiVO_4$ heterostructures. (c) HAADF-STEM image of the $Bi_2O_3/BiVO_4$ heterostructures. (d-f) STEM-EDS elemental mappings of Bi, V and O, respectively.

To study the effect of the p-n heterojunction on the PEC activity of $BiVO_4$ photoanode, PEC measurements were performed on the pristine $BiVO_4$, $Bi_2O_3/BiVO_4$ and Bi_2O_3 samples in a three-electrode electrochemical cell with 0.1 mol L^{-1} Na_2SO_4 solution as the electrolyte. Figure 4a compares the current vs. potential (i-E) curves for the pristine $BiVO_4$, $Bi_2O_3/BiVO_4$ heterostructures and Bi_2O_3 photoelectrodes in the dark and under visible light ($\lambda > 420$ nm) irradiation. As expected, the $Bi_2O_3/BiVO_4$ electrode exhibited the best photocurrent density compared to the $BiVO_4$ and Bi_2O_3. The

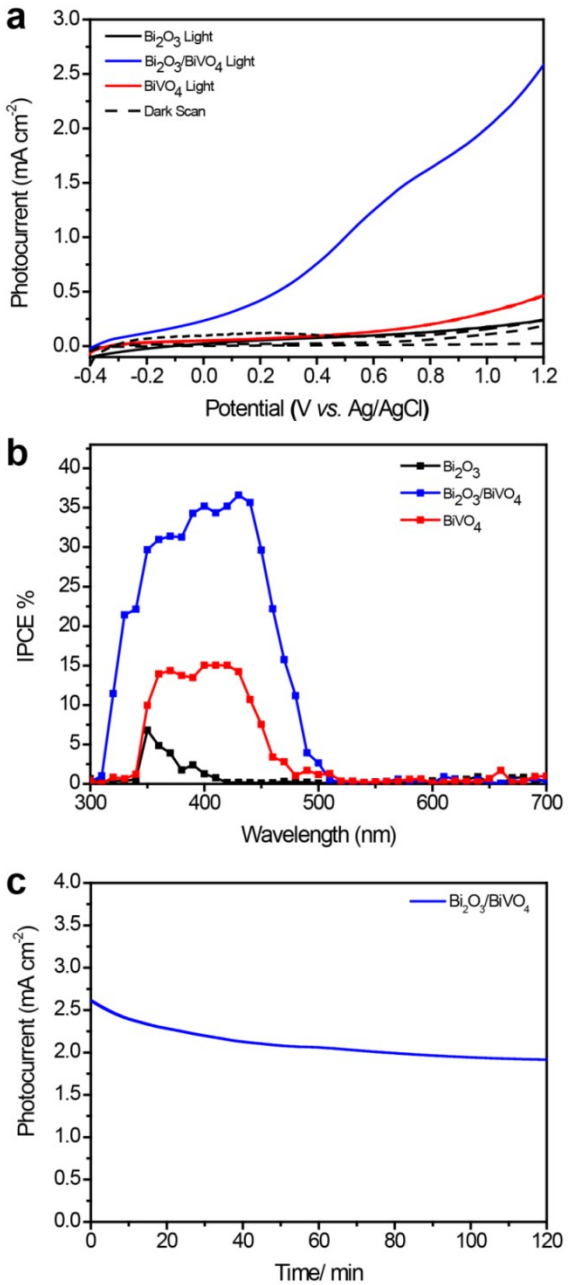

Figure 4. (a) I-E curves recorded with a scan rate of 25 mV s^{-1} under a full-arc xenon lamp irradiation, (b) IPCE spectra collected at the incident wavelength range from 300 to 700 nm at 0.6 V vs. Ag/AgCl of the Bi_2O_3, $BiVO_4$, and $Bi_2O_3/BiVO_4$ heterostructures, (c) Chronoamperometry (*i–t*) of $Bi_2O_3/BiVO_4$ heterostructures.

photocurrent density of $Bi_2O_3/BiVO_4$ achieved a current density of 2.58 mA cm^{-2} at the potential of 1.2 V vs. Ag/AgCl, which is about 5 times higher than those of pristine $BiVO_4$ (0.47 mA cm^{-2}). This present value is also higher than recent reported $BiVO_4$-based photoanodes, such as Co-Pi Modified $BiVO_4$/ZnO (2.0 mA cm^{-2} at 1.2V vs. Ag/AgCl) [31], $WO_3/BiVO_4$ (0.55 mA cm^{-2} at 1.23V vs. Ag/AgCl) [32], $BiVO_4$–TiO_2 (0.53 mA cm^{-2} at 1.2V vs. Ag/AgCl) [25], macro-mesoporous Mo:$BiVO_4$ (2.0 mA cm^{-2} at 1.0 V vs. Ag/AgCl) [33]. Furthermore, the current vs. potential (i-E) curves for the pure p-type Bi_2O_3 is shown in Figure S6. Incident-photon-to-current-conversion efficiency (IPCE) measurements were further performed to investigate the PEC performances of the as-prepared photoelectrodes. Figure 4b shows the IPCE spectra of the pristine Bi_2O_3, $BiVO_4$ and $Bi_2O_3/BiVO_4$ photoelectrodes measured at 0.6 V vs. Ag/AgCl as a function of incident light wavelength. Obviously, the $Bi_2O_3/BiVO_4$ photoanode showed substantially enhanced IPCE values compared to the pristine Bi_2O_3 and $BiVO_4$ at all measured wavelengths, which agree well with their J-V characteristics. The maximum IPCE value of the $Bi_2O_3/BiVO_4$ reaches 35% at 440 nm, which is much higher than that of pristine $BiVO_4$ (about 10% at 440 nm) and pure Bi_2O_3 (about 0.16% at 440 nm). This result conveniently supports our hypothesis that the PEC performance of $BiVO_4$ can be greatly improved by forming $Bi_2O_3/BiVO_4$ p-n type heterostructures.

The PEC stability of a photoelectrode is another crucial point for a PEC cell to produce hydrogen. The stability of the $Bi_2O_3/BiVO_4$ photoanode was also evaluated, and the photocurrent-time (i-t) curves of $Bi_2O_3/BiVO_4$ photoanode collected at 1.2 V vs. Ag/AgCl are shown in Figure 4c. The photocurrent of $Bi_2O_3/BiVO_4$ is initially about 2.58 mA cm^{-2} and the photocurrent only decreases to 2.28 mA cm^{-2} within the initial 20 minutes and then photocurrent decreases slowly to 1.91 mA cm^{-2} within 120 min of illumination. This demonstrates that the $Bi_2O_3/BiVO_4$ heterostructures are very stable during the long time irradiation and extreme voltage, which is due to the separation of electron-hole pairs in the p-n heterostructures.

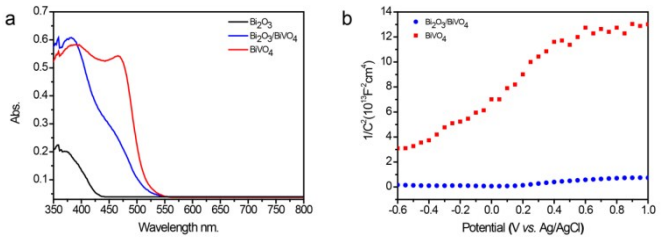

Figure 5. (a) UV-Vis diffuses absorption spectra and (b) Mott-Schottky curves of $BiVO_4$ and $Bi_2O_3/BiVO_4$ heterostructures.

It is known that both the light absorption and separation efficiency of photoexcited electron-hole pairs have important influences on the PEC property of the photoelectrode. Diffuse reflectance UV-visible spectra of the Bi_2O_3, $BiVO_4$ and $Bi_2O_3/BiVO_4$ heterostructures were collected to understand the influence of p-n heterojunction on the light harvesting capability. As shown in Figure 5a, the band edges of the Bi_2O_3 and $BiVO_4$ samples were at about 400 nm and 512 nm, respectively, which are consistent with the recent reports [34, 35]. There is only one absorption band edge as the Bi_2O_3 and $BiVO_4$, distribute so uniformly in the heterostructures, which is consistent with the recent reports, such as $BiOI/TiO_2$ heterostructures,[36] $BiVO_4/TiO_2$ heterostructures[37]. Additionally, the band edge of $Bi_2O_3/BiVO_4$ heterostructures sample (460 nm) lied between the Bi_2O_3 (400 nm) and $BiVO_4$ (512 nm). As an indirect semiconductor, the band gap of

Bi_2O_3, $BiVO_4$ and $Bi_2O_3/BiVO_4$ heterostructures could be determined with the formula:

$$\alpha h\nu = A(h\nu - E_g)^{n/2},$$

where α, h, ν, A, E_g, and n are the absorption coefficient, Planck's constant, the incident light frequency, a constant, the band-gap energy, and an integer, respectively. Among them, n depends on the characteristics of the optical transition in a semiconductor, i.e., direct transition (n = 1) or indirect transition (n = 4). For $BiVO_4$ and Bi_2O_3, both of them pertain to direct transition and the values of n are 1 [38]. The band-gap energy (E_a value) of $BiVO_4$ can be thus estimated from a plot of $(\alpha h\nu)^2$ versus the photon energy ($h\nu$). From the Figure S7, the estimated band gap of Bi_2O_3 sample is about 2.32 eV, which is much smaller than those of untreated $BiVO_4$ (2.36 eV) and Bi_2O_3 (2.85 eV) samples. The conduction band edge of a semiconductor at the point of zero charge can be calculated by the empirical equation:

$$E_{VB} = X - E^e + 0.5E_g \text{ [39]},$$

where E_{VB} is the valence band-edge potential, X is the electronegativity of the semiconductor, expressed as the geometric mean of the absolute electronegativity of the constituent atoms, E^e is the energy of free electrons on the hydrogen scale (about 4.5 eV), E_g is the band-gap energy of the semiconductor, and E_{CB} can be determined by $E_{CB} = E_{VB} - E_g$. The X values for $BiVO_4$ and Bi_2O_3 are ca. 6.04 and 5.95 eV. The band-gap energies of $BiVO_4$ and Bi_2O_3 adopt 2.36 and 2.85 eV, respectively, which are consistent with the recent reports. [34, 35] Given the equation above, the CB and the bottom of the VB of $BiVO_4$ are calculated to be 0.36 and 2.72 eV, the CB and VB of Bi_2O_3 are calculated to be 0.03 and 2.88 eV, respectively. According to the above results, Scheme 1 was proposed to illustrate a possible charge-separation process. The p-type Bi_2O_3 is with Fermi energy level close to the valence band while the n-type $BiVO_4$ is with Fermi energy level close to the conduction band (XPS VBM was shown in Figure S8). When the two semiconductors are in contact, the CB potential of Bi_2O_3 is more negative than that of $BiVO_4$. As shown in Scheme 1, electron−hole pairs will be generated on Bi_2O_3 and $BiVO_4$ under the irradiation of visible-light. The excited holes on the VB of Bi_2O_3 transfer to the CB of $BiVO_4$ and combine together. Then, the electrons produced on the CB of Bi_2O_3 will transfer to Pt electrode to reduce H^+ to form H_2, while the excited holes on the VB of $BiVO_4$ will oxide H_2O to O_2. Furthermore, the migration of photogenerated electrons and holes could be promoted by the internal electric field. Therefore, the formation of $Bi_2O_3/BiVO_4$ p-n heterojunction on the surface could effectively separate the photoexcited electron−hole pairs and could greatly reduce the recombination of the photogenerated charge carries.

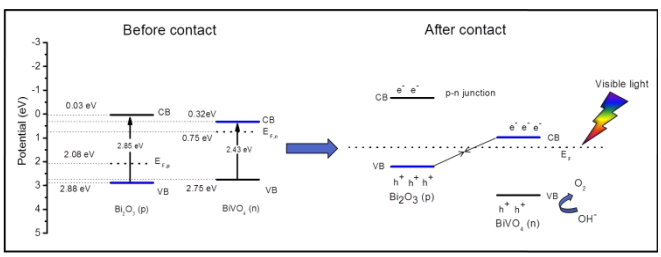

Scheme 1. Schematic diagram of the band energy of Bi_2O_3 and $BiVO_4$ before contact and the formation of a p-n heterojunction and the proposed charge transfer and separation process of $Bi_2O_3/BiVO_4$ p-n heterostructu under visible-light irradiation.

To elucidate the influence of heterostructure on photoelectrical properties of $BiVO_4$, the electrochemical impedance measurements were carried out. Figure 5b shows the Mott-Schottky plots of the $BiVO_4$ electrodes at a frequency of 1 kHz in the dark, which were generated based on capacitances that were derived from the electrochemical impedance. Both the $BiVO_4$ and $Bi_2O_3/BiVO_4$ electrodes show positive slopes, as expected for n-type semiconductors. Notably, $Bi_2O_3/BiVO_4$ shows substantially smaller slope of Mott-Schottky plot compared to bare $BiVO_4$, suggesting significantly increased donor densities based on the following equation:

$$N_d = (2/e_0\varepsilon\varepsilon_0)[d(1/C^2)/dV]^{-1},$$

where N_d is the donor density, e_0 the electron charge, ε the dielectric constant of $BiVO_4$ (ε=86),[20] ε_0 the permittivity of vacuum, and V the applied bias at the electrode. The carrier densities of the $BiVO_4$ and $Bi_2O_3/BiVO_4$ electrodes are calculated to be 1.85×10^{16} and 3.80×10^{17} cm^{-3}, respectively. Notably, $Bi_2O_3/BiVO_4$ electrode possesses one order of magnitude improvement on donor density compared to the bare $BiVO_4$ electrode. The drastically increasing donor density of $Bi_2O_3/BiVO_4$ clearly indicated the enhancement of the conductivity. On the other hand, the Mott-Schottky curve of p-type Bi_2O_3 is shown in Figure S9. All the results clearly verified the assumption that the heterostructures influence the PEC performance deeply.

Conclusions

In summary, the $Bi_2O_3/BiVO_4$ heterostructures were successfully prepared by a simple electrodeposition method and followed calcination. Raman, TEM and XPS analyses confirm the formation of the p-n heterostructures, which can facilitate the transportation and separation of the photo-generated electron-hole pairs. The $Bi_2O_3/BiVO_4$ heterostructures exhibited significantly enhanced PEC activity under visible light irradiation. The photocurrent density of $Bi_2O_3/BiVO_4$ heterostructure photoanode achieved a high photocurrent of 2.58 mA cm^{-2} at 1.2 V vs. Ag/AgCl, which is about 5 times than that of pristine $BiVO_4$. These finding indicates the $Bi_2O_3/BiVO_4$ heterostructures are very promising candidates for PEC cells.

Y.M.Z acknowledges the financial support of this work received by the Natural Science Foundation of China (No. 21276104). K.H.Y acknowledges the Jinan University Scientific Research Innovation Cultivation Project of Excellent Postgraduate Candidates Exempt from Admission Exam (No.33220131114).

Notes and references

[a] Department of Chemistry, Jinan University, Guangzhou 510632, People's Republic China; E-mail: tzhangym@jnu.edu.cn Tel: +86-20-85222756; Fax: +86-20-85222756

[b] Analytic and Testing Centre, Jinan University, Guangzhou, China 510632.

[c] MOE of the Key Laboratory of Bioinorganic and Synthetic Chemistry, KLGHEI of Environment and Energy Chemistry, School of Chemistry and Chemical Engineering, Sun Yat-Sen University, Guangzhou 510275.

Electronic Supplementary Information (ESI) available: [details of any supplementary information available should be included here]. See DOI: 10.1039/c000000x/

1. J. Gan, X. Lu and Y. Tong, *Nanoscale*, 2014, **6**, 7142-7164.
2. X. Lu, S. Xie, H. Yang, Y. Tong and H. Ji, *Chem. Soc. Rev.*, 2014, **43**, 7581-7593.
3. H. G. Kim, P. H. Borse, W. Y. Choi and J. S. Lee, *Angew. Chem. Int. Ed.*, 2005, **44**, 4585-4589.
4. J. Shi, Y. Hara, C. Sun, M. A. Anderson and X. Wang, *Nano Lett.*, 2011, **11**, 3413-3419.
5. X. Lu, G. Wang, S. Xie, J. Shi, W. Li, Y. Tong and Y. Li, *Chem. Commun.*, 2012, **48**, 7717-7719.
6. S. Yang, L. Fan and S. Yang, *J. Phys. Chem. B*, 2004, **108**, 4394-4404.
7. S. Xie, T. Zhai, W. Li, M. Yu, C. Liang, J. Gan, X. Lu and Y. Tong, *Green Chem.*, 2013, **15**, 2434-2440.
8. G. Wang, Y. Ling, H. Wang, X. Lu and Y. Li, *J. Photochem. Photobiology C: Photochem. Rev.*, 2014, **19**, 35-51.
9. S. Xie, T. Zhai, Y. Zhu, W. Li, R. Qiu, Y. Tong and X. Lu, *Int. J. Hydrogen Energy*, 2014, **39**, 4820-4827.
10. C.-H. Zeng, S. Xie, M. Yu, Y. Yang, X. Lu and Y. Tong, *J. Power Sources*, 2014, **247**, 545-550.
11. J. Luo, L. Ma, T. He, C. F. Ng, S. Wang, H. Sun and H. J. Fan, *J. Phys. Chem. C*, 2012, **116**, 11956-11963.
12. K.-H. Ye, J.-Y. Wang, N. Li, Z.-Q. Liu, S.-H. Guo, Y.-P. Guo and Y.-Z. Su, *Inorg. Chem. Commun.*, 2014, **45**, 116-119.
13. H. Li, Y. Fu, H. Liu, M. Zhu, Z. Peng, J. Yang, J. Li, X. Huang, Y. Jiang and Q. Liu, *Inorg. Chem. Commun.*, 2013, **30**, 182-186.
14. C. Yao, B. Wei, H. Ma, L. Meng, X. Zhang and Q. Gong, *J. Power Sources*, 2013, **237**, 295-299.
15. A. Ikram, S. Sahai, S. Rai, S. Dass, R. Shrivastav and V. R. Satsangi, *J. Power Sources*, 2014, **267**, 664-672.
16. H. Li, C. Chen, X. Huang, Y. Leng, M. Hou, X. Xiao, J. Bao, J. You, W. Zhang and Y. Wang, *J. Power Sources*, 2014, **247**, 915-919.
17. T. Wang, J. Tang, S. Wu, X. Fan and J. He, *J. Power Sources*, 2014, **248**, 510-516.
18. M.-L. Guan, D.-K. Ma, S.-W. Hu, Y.-J. Chen and S.-M. Huang, *Inorg. Chem.*, 2011, **50**, 800-805.
19. Y. Liang, T. Tsubota, L. P. A. Mooij and R. van de Krol, *J. Phys. Chem. C*, 2011, **115**, 17594-17598.
20. D. K. Zhong, S. Choi and D. R. Gamelin, *J. Am. Chem. Soc.*, 2011, **133**, 18370-18377.
21. F. F. Abdi and R. van de Krol, *J. Phys. Chem. C*, 2012, **116**, 9398-9404.
22. S. P. Berglund, A. J. E. Rettie, S. Hoang and C. B. Mullins, *Phys. Chem. Chem. Phys.*, 2012, **14**, 7065-7075.
23. Y. Pihosh, I. Turkevych, K. Mawatari, T. Asai, T. Hisatomi, J. Uemura, M. Tosa, K. Shimamura, J. Kubota, K. Domen, *Small*, **10**, 3692-3699.
24. E. Kim, H. Kang, G. Magesh, J. Kim, J. Jang, J. Lee, *ACS Appl. Mater. Interfaces*, 2014, **6**,17762-17769
25. S. Ho-Kimura, S. J. A. Moniz, A. D. Handoko and J. Tang, *J. Mater. Chem. A*, 2014, **2**, 3948-3953.
26. S. Moniz, J. Zhu, J. Tang, *Adv. Energy Mater.*, 2014, **4**, 1301590.
27. L. Li and B. Yan, *J. Alloys Compounds*, 2009, **476**, 624-628.
28. S. K. Pilli, T. E. Furtak, L. D. Brown, T. G. Deutsch, J. A. Turner and A. M. Herring, *Energy Environ. Sci.*, 2011, **4**, 5028-5034.
29. L. Zhang, D. R. Chen and X. L. Jiao, *J. Phys. Chem. B*, 2006, **110**, 2668-2673.
30. Y. Jianqiang and A. Kudo, *Adv. Funct. Mater.*, 2006, **16**, 2163-2169.
31. S. J. A. Moniz, J. Zhu and J. Tang, *Adv. Energy Mater.*, 2014, **4**, 1301590.
32. Y. Pihosh, I. Turkevych, K. Mawatari, T. Asai, T. Hisatomi, J. Uemura, M. Tosa, K. Shimamura, J. Kubota, K. Domen and T. Kitamori, *Small*, 2014, **10**, 3692-3699.
33. M. Zhou, J. Bao, Y. Xu, J. Zhang, J. Xie, M. Guan, C. Wang, L. Wen, Y. Lei and Y. Xie, *ACS Nano*, 2014, **8**, 7088-7098.
34. L. S. Zhang, W. Z. Wang, J. O. Yang, Z. G. Chen, W. Q. Zhang, L. Zhou and S. W. Liu, *Appl. Catal. A-General*, 2006, **308**, 105-110.
35. L. Zhou, W. Wang, L. Zhang, H. Xu and W. Zhu, *J. Phys. Chem. C*, 2007, **111**, 13659-13664.
36. X. Zhang, L. Zhang, T. Xie and D. Wang, *J. Phys. Chem. C*, 2009, **113**, 7371-7378.
37. Y. Hu, D. Li, Y. Zheng, W. Chen, Y. He, Y. Shao, X. Fu and G. Xiao, *Appl. Catal. B: Environ.*, 2011, **104**, 30-36.
38. L. Zhou, W. Z. Wang, S. W. Liu, L. S. Zhang, H. L. Xu and W. Zhu, *J. Molecular Catal. A-Chem.l*, 2006, **252**, 120-124.
39. D. Hou, X. Hu, P. Hu, W. Zhang, M. Zhang and Y. Huang, *Nanoscale*, 2013, **5**, 9764-9772.

Graphical Abstract

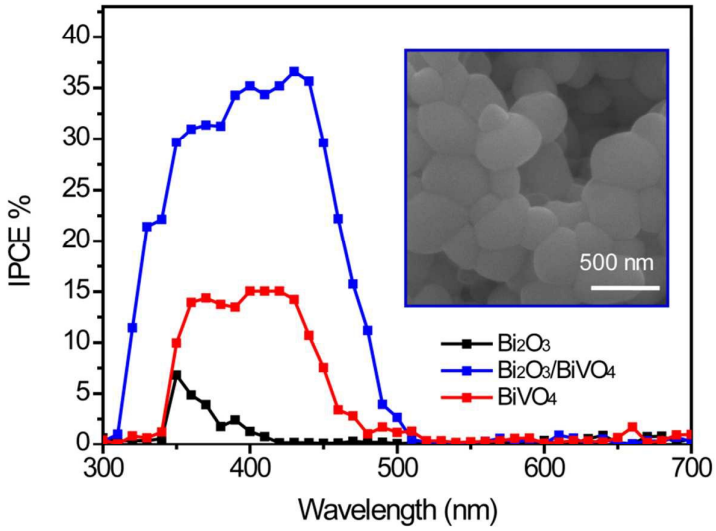

$Bi_2O_3/BiVO_4$ heterostructures with a p-n junction have been successfully synthesized and exhibited enhanced photoelectrochemical activity.